Research Article

Adnan*, Waseem Abbas, Refka Ghodhbani*, Kaouther Ghachem, Tadesse Walelign*, Yasir Khan, Mehdi Akermi, and Rym Hassani

Investigation of solar radiation effects on the energy performance of the $(Al_2O_3–CuO–Cu)/H_2O$ ternary nanofluidic system through a convectively heated cylinder

https://doi.org/10.1515/phys-2025-0177
received June 18, 2024; accepted June 12, 2025

Abstract: Thermal transport in ternary nanofluid is a topic of interest in different engineering systems. These fluids have higher thermal conductivity than traditional nanofluids. Hence, the present study aims to develop a new ternary nanofluid model for a cylindrical working domain. For this, thermophysical properties of ternary nanoliquids and appropriate transformations are used. The problem is then investigated through a numerical approach and the comparative results are obtained. The ternary nanofluid shows an optimum decrease in the velocity due to the involvement of three types of nanoparticles. Suction of the fluid with strength α = 0.1, 0.9, 1.7, 2.5 and Reynolds effects Re = 1.0, 1.5, 2.0, 2.5 significantly control the motion and dominant behaviour is examined for a simple nanofluid. The thermal capability of the nanofluids is enhanced against the concentration factor ϕ_1 = 0.01, 0.0.3, 0.05, 0.07 while suction phenomena resist the temperature. Inclusion of radiations (Rd = 0.1, 0.5, 0.9, 1.3) and convective transport (B_i = 0.01, 0.02, 0.03, 0.04) contribute dominantly for thermal applications in nanofluids. The shear drag magnitude changes from 107.4995 to 162.287% (TNF), 113.427 to 170.666% (HNF), and 120.886 to 180.704% (SNF) for varying ϕ_1 from 1.0 to 7.0%. Further, the efficiency of TNF, HNF, and SNF showed a prominent increase from 42.0126 to 68.8055% (TNF), 40.6019 to 66.6076% (HNF), and 39.8879 to 65.5324% (SNF), for stronger Biot effects from 0.5 to 2.0. Hence, the study's outcomes would help to address the heat transfer issues from multiple aspects.

Keywords: ternary nanofluid, heat transfer, cylinder, thermal radiation, convective surface

*** Corresponding author: Adnan,** Department of Mathematics, Mohi-ud-Din Islamic University, Nerian Sharif, AJ & K, 12080, Pakistan, e-mail: adnan_abbasi89@yahoo.com
*** Corresponding author: Refka Ghodhbani,** Center for Scientific Research and Entrepreneurship, Northern Border University, Arar, 73213, Saudi Arabia, e-mail: refka.ghodhbani@nbu.edu.sa
*** Corresponding author: Tadesse Walelign,** Department of Mathematics, Debre Tabor University, Debre Tabor, Ethiopia, e-mail: tadelenyosy@gmail.com
Waseem Abbas: Department of Mathematics, Mohi-ud-Din Islamic University, Nerian Sharif, AJ & K, 12080, Pakistan
Kaouther Ghachem: Department of Industrial and Systems Engineering, College of Engineering, Princess Nourah bint Abdulrahman University, P.O. Box 84428, Riyadh, 11671, Saudi Arabia
Yasir Khan: Department of Mathematics, University of Hafr Al Batin, Hafr Al Batin, 31991, Saudi Arabia
Mehdi Akermi: Department of Physics Sciences, College of Science, Jazan University, P.O. Box. 114, Jazan, 45142, Kingdom of Saudi Arabia
Rym Hassani: Environment and Nature Research Centre, Jazan University, P.O. Box 114, Jazan 45142, Saudi Arabia

Nomenclature

w, u	components of the velocity (m/s)
p	pressure (Pa)
T, T_∞	fluid temperature and ambient temperature (K)
U_w	surface velocity (m/s)
k_{tnf}	thermal conductivity (W/m K)
ρ_{tnf}	density (kg/m^3)
μ_{tnf}	dynamic viscosity (N s/m^2)
c	arbitrary constant
η	dimensionless variable
F'	velocity dimensionless form
β	temperature dimensionless form
Re	Reynold number
Pr	Prandtl number
Rd	radiation number
B_i	Biot number

Abbreviations

ODEs	ordinary differential equations
PDEs	partial differential equations
MHD	magnetohydrodynamic
TBL	thermal boundary layer

1 Introduction

Improved characteristics of nanomaterials make the primary solvents more realistic for engineering and thermal applications. The researchers made efforts towards the development of these engineered fluids. Mishra [1] scrutinized the importance of Fe_3O_4, $CoFe_2O_4$ nanoparticles' (NPs) impacts on the properties of ethylene glycol (EG). The study was conducted for a permeable surface under two types of slips, termed as Troian and Thompson. The investigation shows that the heat transfer rate decreases absolutely due to the changing parameters. Waqas *et al.* [2] scrutinized that with the greater estimation of the Biot number, the temperature of the fluid is increased. Song *et al.* [3] analyzed an incompressible, time-dependent Williamson nanoliquid flow through a stretching cylinder and observed the reduction in the velocity against the unsteady parameter. Nadeem *et al.* [4] explored the viscoelastic nanofluid [5,6] flow through stretching absorbent media with suction and injection cases. Some recent studies for nanoliquids under varying physical constraints are discussed by various researchers (see refs. [7–9]).

The nanofluid's heat transport mechanism is of greater interest in engineering applications. These fluids are obtained by the dispersion of tiny particles in the traditional fluids. The heat transport rate in a nanoliquid flow under heat dissipative phenomena and heat transfer through a porous cylinder was scrutinized by Waqas *et al.* [2] and concluded that the heat performance enhances the B_i effects increased. Song *et al.* [3] analyzed an incompressible, time-dependent Williamson liquid through a stretching cylinder with the influence of mixed convection and heat transfer effects and observed the reduction in the velocity against unsteady parameter. Nadeem *et al.* [4] explored the viscoelastic nanofluid [5,6] flow through stretching absorbent media for suction and injection cases. Some recent studies for nanoliquids under varying physical constraints are discussed by various researchers (see refs. [10–12]).

Javaid *et al.* [13] studied the dynamics of second-grade fluid past through cylinder placed vertically. They examined the flow nature and heat mechanism comprehensively *via* numerical approach. An unsteady convective flow over a circular cylinder with heating effects is explored by Shah *et al.* [14] by using Fourier's law explained the behavior of velocity and temperature profile against Grashof and Prandtl number. Gholinia *et al.* [15] analyzed an incompressible, viscous mixed convection nanofluid [16,17], flow into a circular vertical cylinder with the influence of electrical conductivity. EG used as a base fluid while NPs included silver and copper in this study. Emam [18] presented an investigation on a steady, boundary layer, incompressible fluid flow over a semi-infinite cylinder which in immersed in the porous medium and move vertically.

Rehman *et al.* [19] performed an analysis of non-Newtonian BL (boundary layer) micropolar liquid with heat transfer into a vertical cylinder which is exponentially stretched and the results of the parameters under consideration are presented through graphs. Ganesh *et al.* [20] examined steady, incompressible, and laminar axi-symmetric boundary layer heat transport over a vertical cylinder influenced by Lorentz forces. They reported that TBL thickness increased with increase in magnetic field parameter and decreased with Prandtl number. Zokri *et al.* [21] discussed the heat transfer due to Grashof effects for Jeffrey nanofluid with heat dissipation effects over a horizontal cylinder.

Javed *et al.* [22] investigated the mixed convective flow of viscous nanofluid [23,24] with the effects of constant heat flux over an elliptical cylinder and concluded that Skin friction and Nusselt number increased with growing value mixed convection parameter. Similarly, a free convection boundary layer nanofluid flow with constant temperature over an elliptical cylinder with the impact of Brownian motion was securitized in a study by Cheng [25]. An MHD mixed convective flow of a ternary nanofluid consisting on NPs, including Cu, Al_2O_3, and TiO_2 due to inner rotating cylinder was examined by Lahonian *et al.* [26]. Recently, Noreen *et al.* [27] recognized the CCM to express an MHD ternary nanofluid flow model by considering heating source and magnetic field effects through double discs.

Recently, researcher's community inspired by the characteristics of advanced nanofluids and accelerated towards the analysis in this new direction. Mohanty *et al.* [28] discussed irreversibility characteristics of ternary nanofluids through an elastic cylinder and pointed there industrial uses. They included resistive heating and solar radiations of nonlinear nature to upsurges the novelty. The study revealed that ternary nanofluid prepared by MWCNTs, SWCNTs, and GO are efficient than the previously discussed nanofluids. Sarangi *et al.* [29] explored the performance of Bodewadt flow a fluid containing ternary NPs. The study accommodated the effects of stretching, dissipation, and radiations for the flow situation over a disk. Reduced surface drag due to

ternary NPs, and minimized entropy of the system for smaller thermal differences are the main findings. Analysis of combined convection, permeability, and activation energy has been conducted by Mohanty *et al.* [30]. It is noticed that Sherwood number declines due to augmenting chemical and activation energy effects.

Pandey and Kumar [31] explored the collective impact of thermal radiation and convection flow of nanofluid consisting on Cu NPs and considered viscous dissipation past a porous stretching cylinder and discussed the Nusselt number against the various physical constraints. The viscous dissipation and heat transfer nanofluid flow with non-thermal radiations over a cylinder with radiations is examined in [32]. Mehmood *et al.* [33] investigated the transport of NPs [34,35] aluminum oxide in EG past a convectively heated cylinder. Heat performance rate of ternary nanofluid over a permeable cylinder is comprehensibly investigated in [36] with the effects of permeable medium, inclined geometry and heat source/sink on temperature distribution.

Fractional order approaches [37] and ANN schemes [38] are newly introduced mathematical tools for the analysis of nanofluid problems. Researchers put their efforts for the investigate nanofluids dynamics under varying controls and geometries for remarkable thermal transport using these schemes. Khan *et al.* [39], examined nanofluid inspired by the influences of an MHD in darcy media. The nonlinear problem discussed through fractional order derivative approach and comprehensively elaborated the outputs. The 56.51% increase in the temperature is acquired for Grashof effects and suggested that tackled issue is good to cope the problems of combustion engines, and maintaining temperature of electronic devices. Another relevant study by introducing the γ nanoliquid has been reported in [40]. The γAl_2O_3 NPs utilized to augment the characteristics of H_2O and $C_2H_6O_2$ along with adopted physical controls. They examined that $\gamma Al_2O_3(C_2H_6O_2)$ is better to $\gamma Al_2O_3(H_2O)$ from applications perspectives in power plants, turbines and heat exchanging devices.

This novelty and objectives of this research falls in three steps. Firstly, prolong the traditional problem for ternary nanofluids which has promising features than hybrid or conventional nanofluids. This will spotlight the importance of composition of three types of NPs for heat featuring applications. Secondly, to investigate the impacts on radiations and suction on the comparative efficiency of ternary, hybrid and simple fluids performance. Thirdly, to introduce the convective condition and how it alter the behaviour of nanofluids through a cylinder and its impacts on the rate of heat transfer. The comparative study of three sort of nanofluids would help to predict the type of nanofluids for superior thermal applications and control of shear drag and rate of thermal transport. This will add valuable insights in the engineering and heat transfer applications.

2 Model development

Suppose an incompressible and steady nature flow of ternary nanofluid through a cylinder. The fluid components

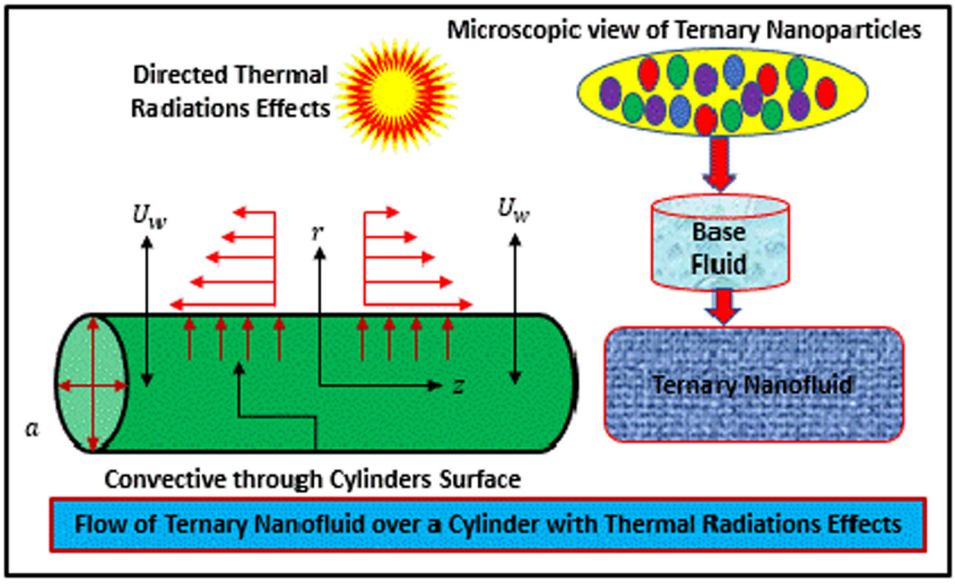

Figure 1: Incompressible ternary nanofluid flow through a cylinder.

are Cu, CuO, and Al_2O_3, while water is taken as the primary solvent. Further, a be the radius along the extending axial direction, r makes a right angle with the z-axis, and the z-axis is parallel to the cylinder. The suction effects on the cylinder. The whole flow situation is configured in Figure 1, while the supporting governing laws for the continuity, momentum, and energy are given in Eqs. (1)–(6) along with fitting flow conditions [2]

$$\frac{\partial}{\partial r}(ru) + \frac{\partial}{\partial z}(rw) = 0, \tag{1}$$

$$\rho_{\text{tnf}}\left(u\frac{\partial u}{\partial r} + w\frac{\partial u}{\partial z}\right) = \left[-\frac{u}{r^2} + \frac{\partial^2 u}{\partial r^2} + \frac{1}{r}\frac{\partial u}{\partial r}\right]\mu_{\text{tnf}}, \tag{2}$$

$$\rho_{\text{tnf}}\left(u\frac{\partial w}{\partial r} + w\frac{\partial w}{\partial z}\right) = \left[\frac{\partial^2 w}{\partial r^2} + \frac{1}{r}\frac{\partial w}{\partial r}\right]\mu_{\text{tnf}}, \tag{3}$$

$$(\rho c_{\text{p}})_{\text{tnf}}\left(w\frac{\partial T}{\partial z} + u\frac{\partial T}{\partial r}\right) = k_{\text{tnf}}\left[\frac{\partial^2 T}{\partial r^2} + \frac{1}{r}\frac{\partial T}{\partial r}\right] + \frac{\partial}{\partial r}\left[\frac{16\sigma^* T_\infty^3}{3k^*}\frac{\partial T}{\partial r}\right]. \tag{4}$$

The above equations are associated with the boundary conditions as follows:

$$r \to \infty : \quad T \to T_\infty, \quad w \to 0, \tag{5}$$

$$r = a : \quad -k_{\text{tnf}}\frac{\partial T}{\partial r} = h_{\text{f}}(T_{\text{f}} - T), \quad w = w_{\text{w}}, \quad u = U_{\text{w}}. \tag{6}$$

Here, $U_{\text{w}} = -aac$ and $w_{\text{w}} = 2zc$.

The following ternary nanoliquid [41,42] models are preferred to check the performance of the ternary nanoliquid. The ternary NPs (Al_2O_3–CuO–Cu) are taken, which are uniformly dissolved in the host liquid. The detailed expressions for improved properties of ternary nanoliquids are described in Table 1. It is noteworthy that these models easily reduced for the previous classes (hybrid and nanofluids) by setting the concentration factor. Figure 2a–c shows the thermo-physical properties of various NPs and base fluid involved in this study. Further, Figure 3a–d present the impacts of NPs changing concentration on the effective properties.

To convert the basic model into final form, we introduced the following velocity and temperature variables, which support the current analysis

$$u = -ac[\eta^{-0.5}F(\eta)], \eta = \left(\frac{r}{a}\right)^2, \beta(\eta) = \frac{T - T_\infty}{T_{\text{f}} - T_\infty}, \quad w = 2zcF'(\eta). \tag{7}$$

In the next stage, the desired model is achieved by implementing the appropriate differentiation and ternary nanoliquid formulas in the primary governing laws:

$$\eta F''' + F'' - \rho_{\frac{\text{tnf}}{\rho_{\text{f}}}}\left(\frac{\mu_{\text{tnf}}}{\mu_{\text{f}}}\right)^{-1}\text{Re}(F'^2 - FF'') = 0, \tag{8}$$

$$2(\eta\beta'' + \beta') + \frac{(\rho C\text{p})_{\text{tnf}}}{(\rho c_{\text{p}})_{\text{f}}}\left(\frac{k_{\text{tnf}}}{k_{\text{f}}}\right)^{-1}\text{Pr Re}F\beta' + \text{Rd}(2\eta\beta'' + \beta') = 0. \tag{9}$$

Moreover, the conditions imposed on the velocity and temperature of the ternary nanoliquid over a cylinder are reduced in the subsequent equations

$$F(1) = \alpha, \quad F'(1) = 1, \quad F'(\infty) \to 0, \tag{10}$$

Table 1: The enhanced characteristics of ternary nanoliquids

Enhanced characteristics	Supporting model
Density	$\rho_{\text{tnf}} = \tilde{\zeta}_3\left[\tilde{\zeta}_2\left\{\tilde{\zeta}_1 + \varphi_1\frac{\rho_{s_1}}{\rho_{\text{f}}}\right\} + \varphi_2\frac{\rho_{s_2}}{\rho_{\text{f}}}\right]\varphi_3\frac{\rho_{s_3}}{\rho_{\text{f}}}$
	$\tilde{\zeta}_1 = 1 - \varphi_1, \ \tilde{\zeta}_2 = 1 - \varphi_2, \ \tilde{\zeta}_3 = 1 - \varphi_3$
Dynamic viscosity	$\mu_{\text{tnf}} = \frac{1}{\tilde{\zeta}_1^{2.5}\tilde{\zeta}_2^{2.5}\tilde{\zeta}_3^{2.5}}$
	$\tilde{\zeta}_1 = 1 - \varphi_1, \ \tilde{\zeta}_2 = 1 - \varphi_2, \ \tilde{\zeta}_3 = 1 - \varphi_3$
Heat capacity	$(\rho C_{\text{p}})_{\text{tnf}} = (\rho C_{\text{p}})_f\left[\tilde{\zeta}_3\left[\tilde{\zeta}_2\left\{\tilde{\zeta}_1 + \varphi_1\frac{(\rho C_{\text{p}})_{s_1}}{(\rho C_{\text{p}})_{\text{f}}}\right\} + \varphi_2\frac{(\rho C_{\text{p}})_{s_2}}{(\rho C_{\text{p}})_{\text{f}}}\right] + \varphi_3\frac{(\rho C_{\text{p}})_{s_3}}{(\rho C_{\text{p}})_{\text{f}}}\right]$
Thermal conductivity	$\frac{\tilde{k}_{\text{tnf}}}{\tilde{k}_{\text{hnf}}} = \frac{\tilde{k}_{s_3} + 2\tilde{k}_{\text{hnf}} - 2\varphi_3(\tilde{k}_{\text{hnf}} - \tilde{k}_{s_3})}{\tilde{k}_{s_3} + 2\tilde{k}_{\text{hnf}} + \varphi_3(\tilde{k}_{\text{hnf}} - \tilde{k}_{s_3})}$
	$\frac{\tilde{k}_{\text{hnf}}}{\tilde{k}_{\text{nf}}} = \frac{\tilde{k}_{s_2} + 2\tilde{k}_{\text{nf}} - 2\varphi_2(\tilde{k}_{\text{nf}} - \tilde{k}_{s_2})}{\tilde{k}_{s_2} + 2\tilde{k}_{\text{nf}} + \varphi_2(\tilde{k}_{\text{nf}} - \tilde{k}_{s_2})}$
	$\frac{\tilde{k}_{\text{nf}}}{\tilde{k}_{\text{f}}} = \frac{\tilde{k}_{s_1} + 2\tilde{k}_{\text{f}} - 2\varphi_1(\tilde{k}_{\text{f}} - \tilde{k}_{s_1})}{\tilde{k}_{s_1} + 2\tilde{k}_{\text{f}} + \varphi_1(\tilde{k}_{\text{f}} - \tilde{k}_{s_1})}$

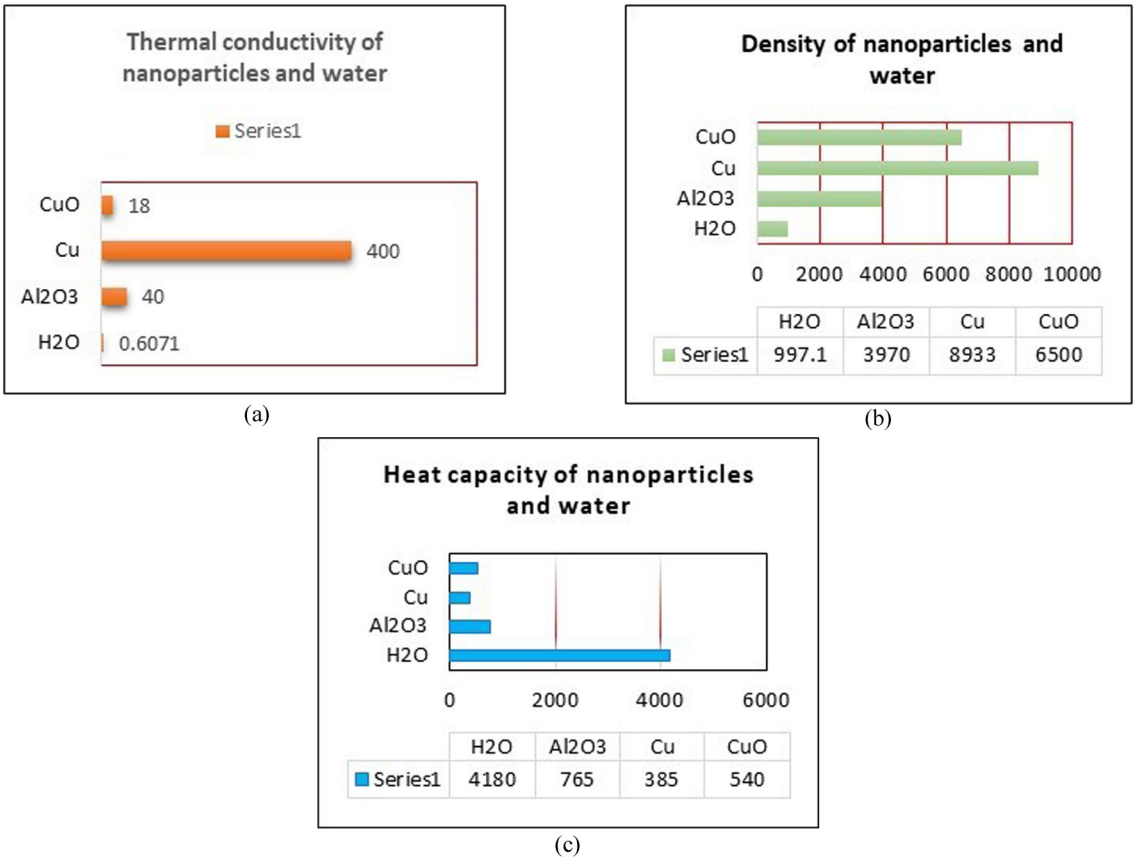

Figure 2: Thermal–physical properties of the components in (a)–(c).

$$\frac{\tilde{k}_{\text{tnf}}}{\tilde{k}_{\text{f}}}\beta'(1) = -B_i(1-\beta(1)), \beta(\infty) = 0, \tag{11}$$

where $\text{Pr} = \frac{\mu_{\text{f}}(C_{\text{p}})_{\text{f}}}{k_{\text{f}}}$ is the Prandtl number, $\text{Re} = \frac{a^2 c}{\nu_{\text{f}}}$ is the Reynolds number, $\text{Rd} = \frac{16\sigma^* T_\infty^3}{3k^* k_{\text{f}}}$ is the radiation parameter, and $B_i = \frac{a^2 h_{\text{f}}}{2rk_{\text{f}}}$ is the Biot number and the suction parameter, respectively. Moreover, φ_1, φ_2, and φ_3 represent the NPs concentration.

The study of shear drag and heat transport rate at the working surface are important factors in many engineering systems. Therefore, these expressions for ternary nanofluids flow through a cylinder are described in Eqs. (12) and (13), respectively

$$C_{\text{f}} = \frac{\tau_{\text{w}}}{\frac{1}{2}\rho_{\text{tnf}} u_{\text{w}}^2} \text{ and } \text{Nu} = \frac{rQ_{\text{w}}}{k_{\text{f}}(T_{\text{w}} - T_\infty)}, \tag{12}$$

where

$$\tau_{\text{w}} = \mu_{\text{tnf}}\left(\frac{\partial u}{\partial r}\right), \text{ and } Q_{\text{w}} = -\left[\left(k_{\text{tnf}} + \frac{16\sigma^* T_\infty^3}{3k^*}\right)\frac{\partial T}{\partial r}\right] \text{ at } r = a. \tag{13}$$

Now, the final expression for shear drag and heat transfer rate is

$$C_{\text{f}} = \left[\left(\frac{\frac{\mu_{\text{tnf}}}{\mu_{\text{f}}}}{\frac{\rho_{\text{tnf}}}{\rho_{\text{f}}}}\right)F''(1)\right] \text{ and } \text{Nu} = -2\left(\frac{k_{\text{tnf}}}{k_{\text{f}}} + \text{Rd}\right)\beta'(1). \tag{14}$$

3 Mathematical analysis

As the scientific problems are mostly modeled with the help of appropriate partial differential equations [43] or non-linear ordinary differential equations (ODEs) along with specific boundary conditions. The ternary nanofluid

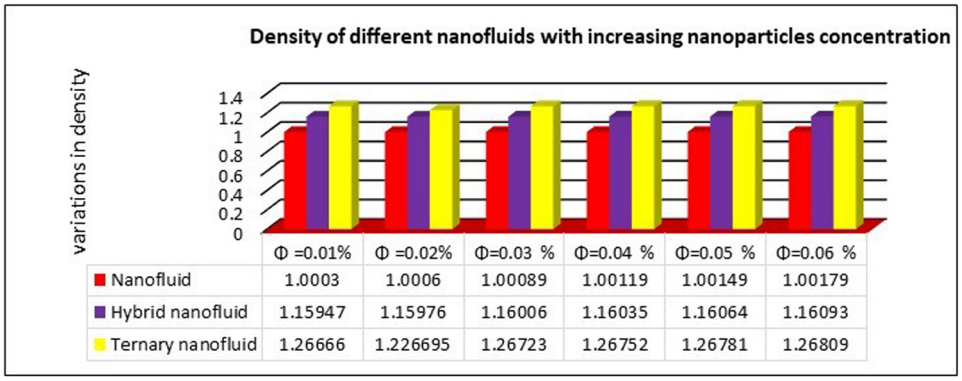

	Φ =0.01%	Φ =0.02%	Φ=0.03 %	Φ=0.04 %	Φ=0.05 %	Φ=0.06 %
Nanofluid	1.0003	1.0006	1.00089	1.00119	1.00149	1.00179
Hybrid nanofluid	1.15947	1.15976	1.16006	1.16035	1.16064	1.16093
Ternary nanofluid	1.26666	1.226695	1.26723	1.26752	1.26781	1.26809

(a)

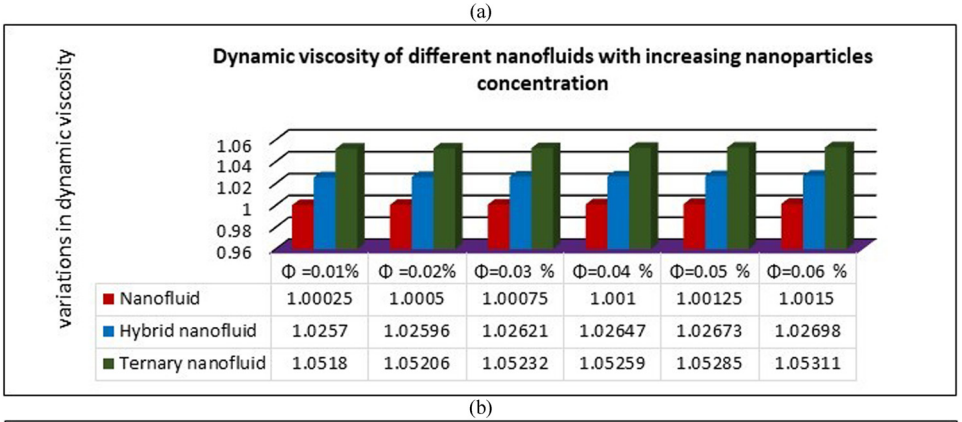

	Φ =0.01%	Φ =0.02%	Φ=0.03 %	Φ=0.04 %	Φ=0.05 %	Φ=0.06 %
Nanofluid	1.00025	1.0005	1.00075	1.001	1.00125	1.0015
Hybrid nanofluid	1.0257	1.02596	1.02621	1.02647	1.02673	1.02698
Ternary nanofluid	1.0518	1.05206	1.05232	1.05259	1.05285	1.05311

(b)

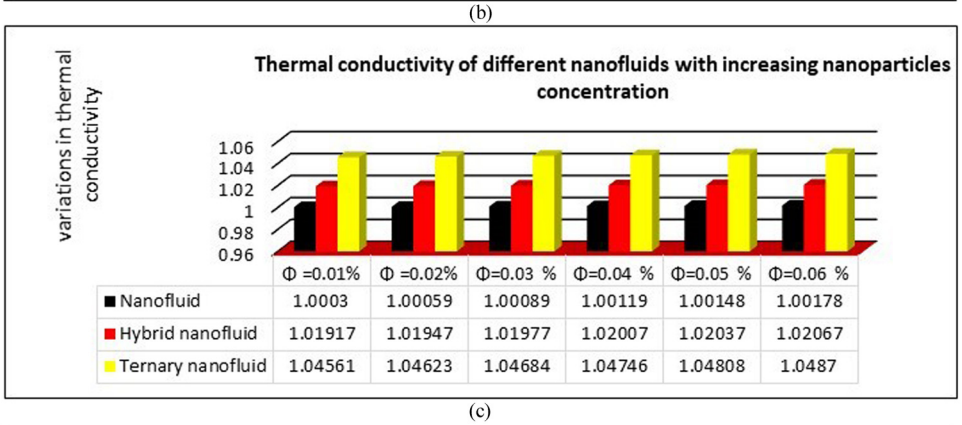

	Φ =0.01%	Φ =0.02%	Φ=0.03 %	Φ=0.04 %	Φ=0.05 %	Φ=0.06 %
Nanofluid	1.0003	1.00059	1.00089	1.00119	1.00148	1.00178
Hybrid nanofluid	1.01917	1.01947	1.01977	1.02007	1.02037	1.02067
Ternary nanofluid	1.04561	1.04623	1.04684	1.04746	1.04808	1.0487

(c)

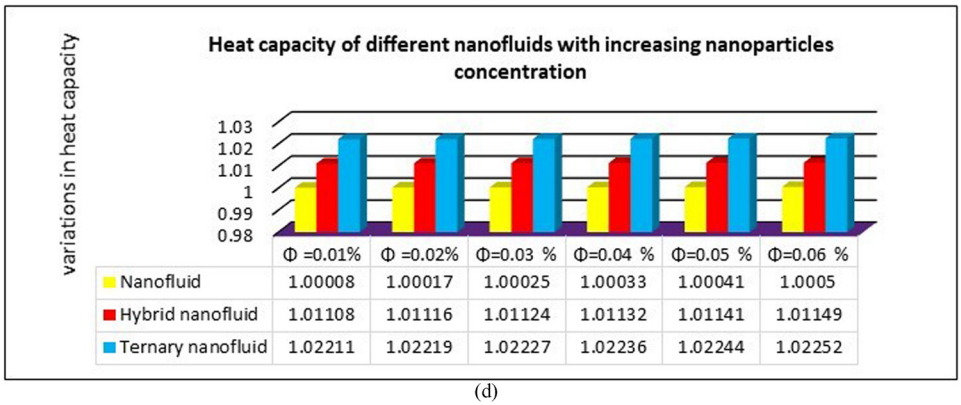

	Φ =0.01%	Φ =0.02%	Φ=0.03 %	Φ=0.04 %	Φ=0.05 %	Φ=0.06 %
Nanofluid	1.00008	1.00017	1.00025	1.00033	1.00041	1.0005
Hybrid nanofluid	1.01108	1.01116	1.01124	1.01132	1.01141	1.01149
Ternary nanofluid	1.02211	1.02219	1.02227	1.02236	1.02244	1.02252

(d)

Figure 3: Comparison of nanofluids characteristics against the increasing weight concentration in (a)–(d).

model, developed in this study, is necessary to solve for the description of a flow phenomenon against various physical constraints. The governing equations develop in the model are first reduced into system of ODEs.

Step I: Introduce the velocity and temperature transformative functions against the model order as given in Eqs. (8) and (9)

$$\breve{\Theta}_{l1} = F, \breve{\Theta}_{l2} = F', \breve{\Theta}_{l3} = F'', \breve{\Theta}'_{l3} = F''', \tag{15}$$

$$\breve{\Theta}_{l4} = \beta, \breve{\Theta}_{l5} = \beta', \breve{\Theta}'_{l5} = \beta''. \tag{16}$$

Step II: Rearrangement of the problem is carried out in this step for the insertion of the functions from Eqs. (15) and (16)

$$\eta F''' = -F'' + \rho_{\frac{\text{tnf}}{\text{f}}}\left(\frac{\mu_{\text{tnf}}}{\mu_{\text{f}}}\right)^{-1} \text{Re}(F'^2 - FF'') \tag{17}$$

$$F''' = \frac{1}{\eta}\left[-F'' + \rho_{\frac{\text{tnf}}{\text{f}}}\left(\frac{\mu_{\text{tnf}}}{\mu_{\text{f}}}\right)^{-1} \text{Re}(F'^2 - FF'')\right], \tag{18}$$

$$2(\eta\beta'' + \beta') = -\frac{(\rho C_{\text{p}})_{\text{tnf}}}{(\rho c_p)_{\text{f}}}\left(\frac{k_{\text{tnf}}}{k_{\text{f}}}\right)^{-1} \text{Pr Re}F\beta' - \text{Rd}(2\eta\beta'' + \beta'), \tag{19}$$

$$2(\eta\beta'') = -\frac{(\rho C_{\text{p}})_{\text{tnf}}}{(\rho c_{\text{p}})_{\text{f}}}\left(\frac{k_{\text{tnf}}}{k_{\text{f}}}\right)^{-1} \text{Pr Re}F\beta' - \text{Rd}(2\eta\beta'' + \beta') - 2\beta', \tag{20}$$

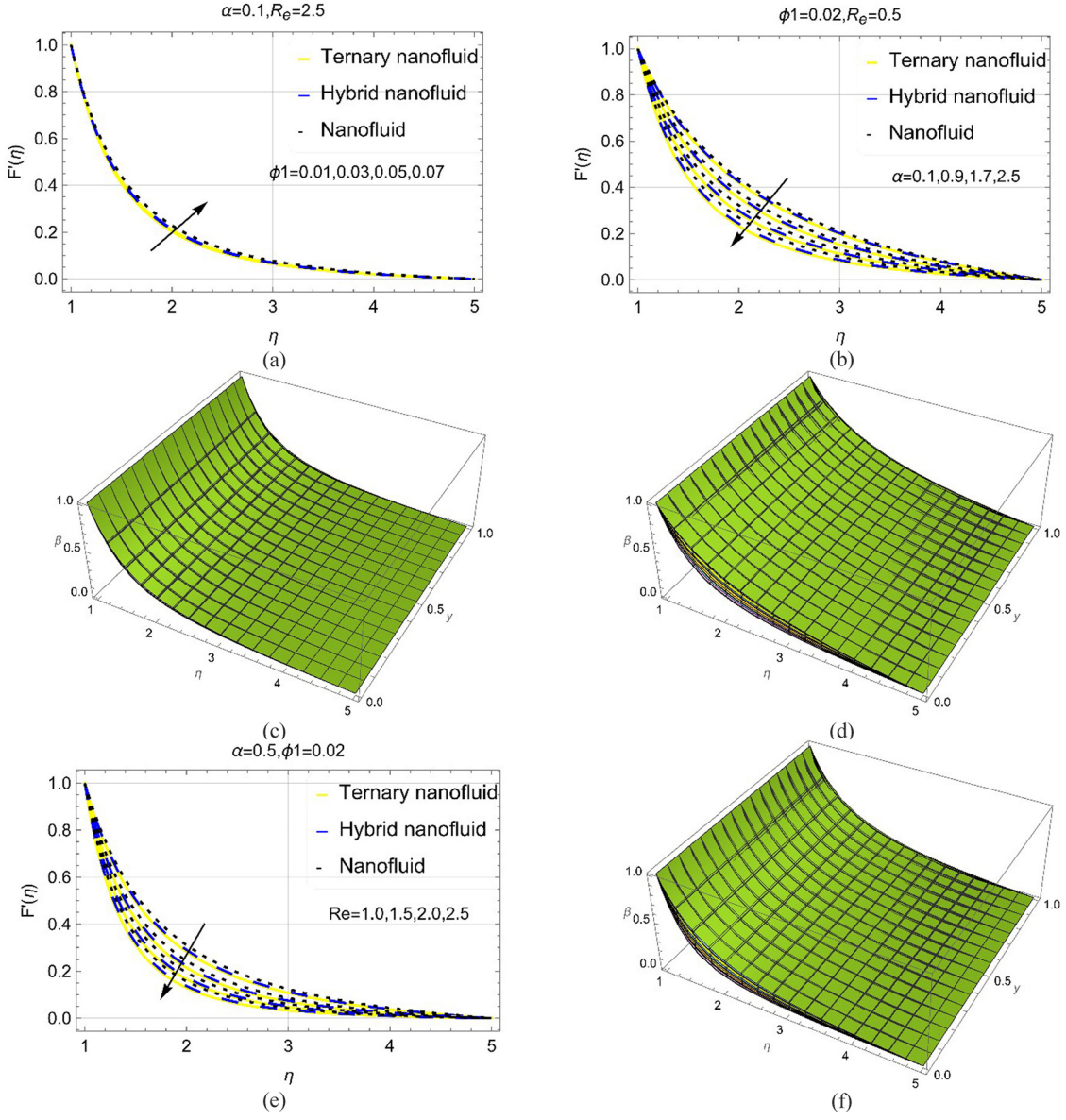

Figure 4: The velocity performance for the mentioned constraints in (a)–(f).

$$(\beta'') = \frac{1}{2\eta}\left[-\frac{(\rho C_p)_{tnf}}{(\rho c_p)_f}\left(\frac{k_{tnf}}{k_f}\right)^{-1} \mathrm{Pr}\,\mathrm{Re} F\beta' - \mathrm{Rd}(2\eta\beta'' + \beta') - 2\beta'\right]. \quad (21)$$

Step III: Reduce Eqs. (18) and (21) as follows using Eqs. (15) and (16), respectively

$$\check{\Theta}'_{l3} = \frac{1}{\eta}\left[-\check{\Theta}_{l3} + \rho_{\frac{tnf}{\rho_f}}\left(\frac{\mu_{tnf}}{\mu_f}\right)^{-1} \mathrm{Re}((\check{\Theta}_{l2})^2 - \check{\Theta}_{l1}\check{\Theta}_{l3})\right], \quad (22)$$

$$\check{\Theta}'_{l5} = \frac{1}{2\eta}\left[-\frac{(\rho C_p)_{tnf}}{(\rho c_p)_f}\left(\frac{k_{tnf}}{k_f}\right)^{-1} \mathrm{Pr}\,\mathrm{Re}\check{\Theta}_{l1}\check{\Theta}_{l5} - \mathrm{Rd}(2\eta\check{\Theta}'_{l5} + \check{\Theta}_{l5}) - 2\check{\Theta}_{l5}\right]. \quad (23)$$

Step IV: In this step, the transformed problem in Eqs. (22) and (23) is analyzed using MATHEMATICA 13.0 and the output results are obtained. The convergence of the scheme is subject to the satisfaction of the conditions and asymptotic behavior.

4 Results and discussion

This section contains a comprehensive discussion of the results under varying levels of the physical parameters. These are shown in Figures 4–6 for the temperature.

Figure 4 shows the velocity trends for ϕ_1, α, and Reynolds number. The investigation reveals that the velocity fluctuation is very slow for increasing values of ϕ_1. Physically, the density of primary fluid enhances when the NPs amount increases from 0.01 to 0.07. Due to increase density, the mass per unit volume increases, which directly affects the movement of the ternary nanofluid. Further, the mass suction results drop in the velocity as shown in Figure 4b for all types of fluids under consideration. Physically, the mass suction through the surface attracts the fluid molecules outside the fluidic system, which reduces the momentum; as a consequence, the movement declines. The velocity approaches zero, which fulfills the flow condition far from the working domain. In nanofluid, the reduction in the velocity is slower than in hybrid and ternary fluids because this is less dense than the other two types, which allow the free movement. Moreover,

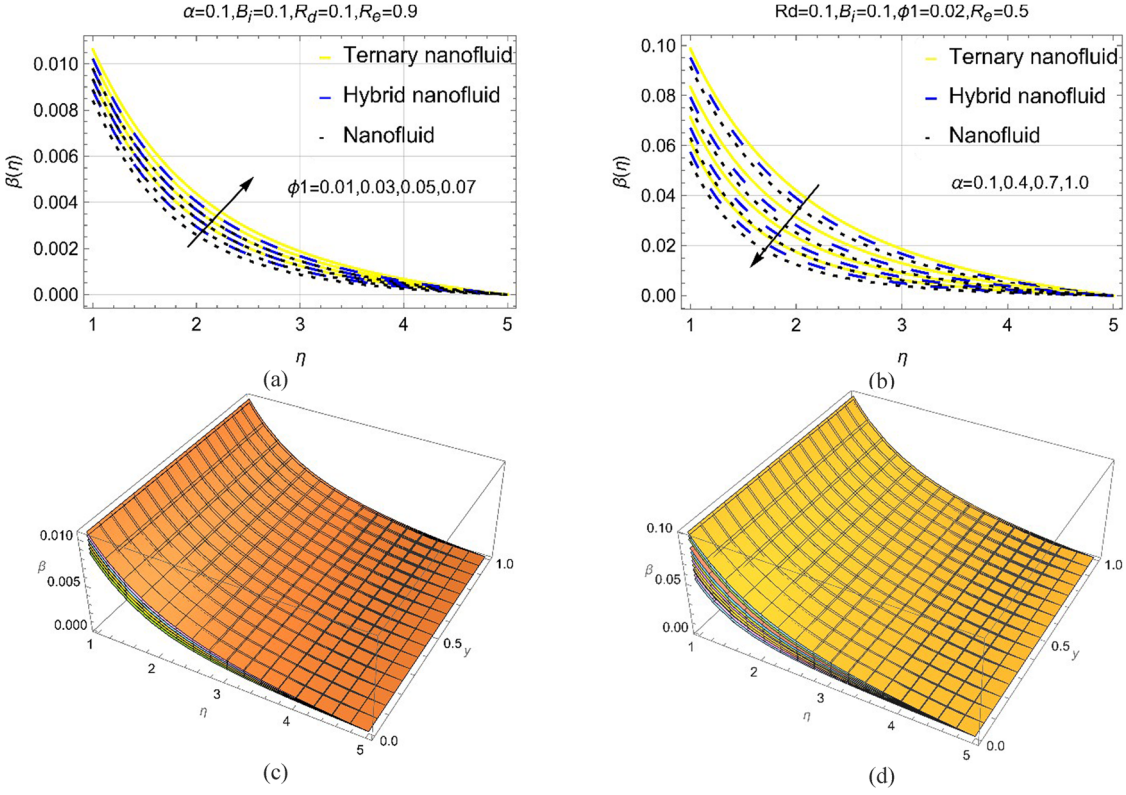

Figure 5: The temperature performance against the mentioned constraints in (a)–(d).

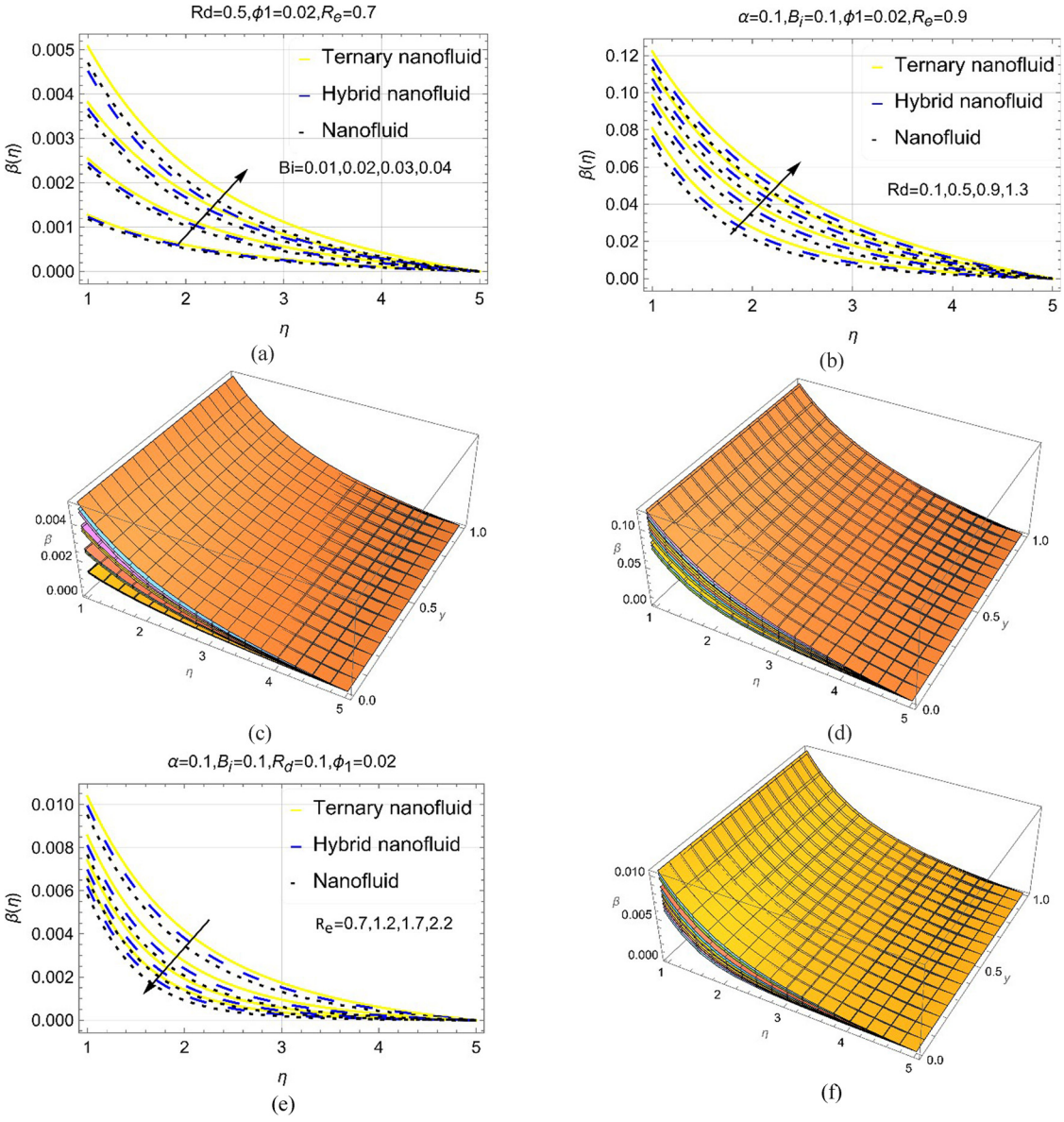

Figure 6: The temperature efficiency for B_i, Rd, and Re in (a)–(f).

the larger Re values is observed to control the motion in the current scenario.

The changes in the physical parameters alter the efficiency of the flow of fluid through a cylinder. Hence, Figures 5 and 6 are organized to analyze the temperature fluctuations in ternary, nano, and hybrid nanofluids against the mentioned ranges of the parameters. The temperature in all three types of nanofluids was augmented for ϕ_1 = 1.0% to ϕ_1 = 7%, while the mass suction effects depreciate it. The prominent change in the temperature due to ϕ_1 is associated with the thermal conductivity difference of these fluids. Physically, the simple nanofluid has the lowest thermal conductivity due to the role of only one type of nanoparticle. Due to this, the heat transfer ability of simple nanofluid is weaker than hybrid and ternary nanofluids. These results along with their 3D scenarios are shown in Figure 5a–d, respectively.

The two heat transfer ways, solar radiation and convective conditions, are of utmost interest in the study of nanofluids. Figure 6a–d illustrates the performance of nanofluids when B_i changes from 0.01 to 0.04 and radiation number Rd from 0.1 to 1.3. It is scrutinized that both these two factors are crucial for heat transfer applications. Physically, imposed radiation effects augment the internal energy of the system, due to which the performance of the whole system enhances. Further, the convective

Table 2: Shear drag computation for multiple model quantities

Parametric ranges			Comparative shear drag for nanofluids		
φ_1	Re	α	Ternary nanoliquid	Hybrid nanoliquid	Nanoliquid
0.01			−0.57500	−0.61443	−0.67097
0.03			−0.57427	−0.61420	−0.67139
0.05			−0.57334	−0.61371	−0.67148
0.07			−0.57223	−0.61299	−0.67128
0.02	1.0		−1.07499	−1.13427	−1.20886
	1.5		−1.27963	−1.34795	−1.43190
	2.0		−1.45964	−1.53605	−1.62856
	2.5		−1.62287	−1.70666	−1.80704
	0.1	1.0	−0.61689	−0.65765	−0.71493
		1.5	−0.64127	−0.68262	−0.74005
		2.0	−0.66630	−0.70822	−0.76577
		2.5	−0.69198	−0.73447	−0.79209

condition shows dominant changes in the temperature near the surface of the cylinder. Physically, near the surface, conduction takes place, which heats up the particles near the surface. These particles gain energy due to the heated surface and move towards the free stream, and the other particles take their place. Due to this continuous process, the temperature significantly enhances near the surface. Further, Figure 6e and f reveal that the increasing ranges of Re are good to the temperature depreciation.

Tables 2 and 3 present the numeric computation of the skin friction and heat gradient. The fluctuation of shear drag against numerous values of φ_1, Re, and α for ternary, hybrid, and simple nanofluid flow is computed in Table 2. For φ_1, Re, and suction parameter α, the skin friction is greater for the ternary nanofluid than for the other two types. Physically, the ternary fluid has dominant denser effects due to which the shear drag is higher than hybrid and simple nanofluids. Hence, the skin friction coefficient gradually decreases from ternary to simple fluids. Moreover, the value of C_f slightly increases for all three nanofluids with increasing value of φ_1.

Table 3 reveals that the thermal radiation parameter is increasing the Nu values. When the value of the radiation parameter Rd is increased, the TC of the nanoliquid is also enhanced. As, the particle's strength in ternary nanofluid is larger than hybrid nanofluid, which has a greater concentration value as compared to the hybrid and common nanofluids. On the basis of weight concentration, the temperature of the ternary nanofluid rises more rapidly than hybrid nanofluid. That is why, with the increase in radiation parameter, the value of Nu is larger.

The involved constraints in the study greatly affect the flow and heat lines patterns. Thus, Figure 7a–h are furnished for different values of the physical controls and found that the stream contours are thick along the vertical axis. Further, the heatline contours are examined less at

Table 3: Comparative computation for heat transfer rate against the model parameters

Model quantities					Computation for heat transfer rate		
φ_1	Re	α	Rd	B_i	Ternary	Hybrid	Nano
0.01					0.140929	0.136004	0.133445
0.03					0.140699	0.135765	0.133198
0.05					0.140495	0.135552	0.132977
0.07					0.140312	0.135362	0.132779
0.02	1.0				0.149639	0.144708	0.142235
	1.5				0.151668	0.146644	0.144112
	2.0				0.153016	0.147912	0.145324
	2.5				0.153987	0.148816	0.146183
	0.1	1.0			0.143328	0.138461	0.135972
		1.5			0.144559	0.13971	0.137245
		2.0			0.145684	0.140842	0.138391
		2.5			0.146711	0.141869	0.139425
		1.5	0.5		0.141668	0.136891	0.134458
			1.0		0.139295	0.13456	0.132139
			1.5		0.137697	0.132983	0.130563
			2.0		0.136552	0.13185	0.129428
			1.0	0.5	0.420126	0.406019	0.398879
				1.0	0.567431	0.548888	0.53967
				1.5	0.642526	0.621823	0.611632
				2.0	0.688055	0.666076	0.655324

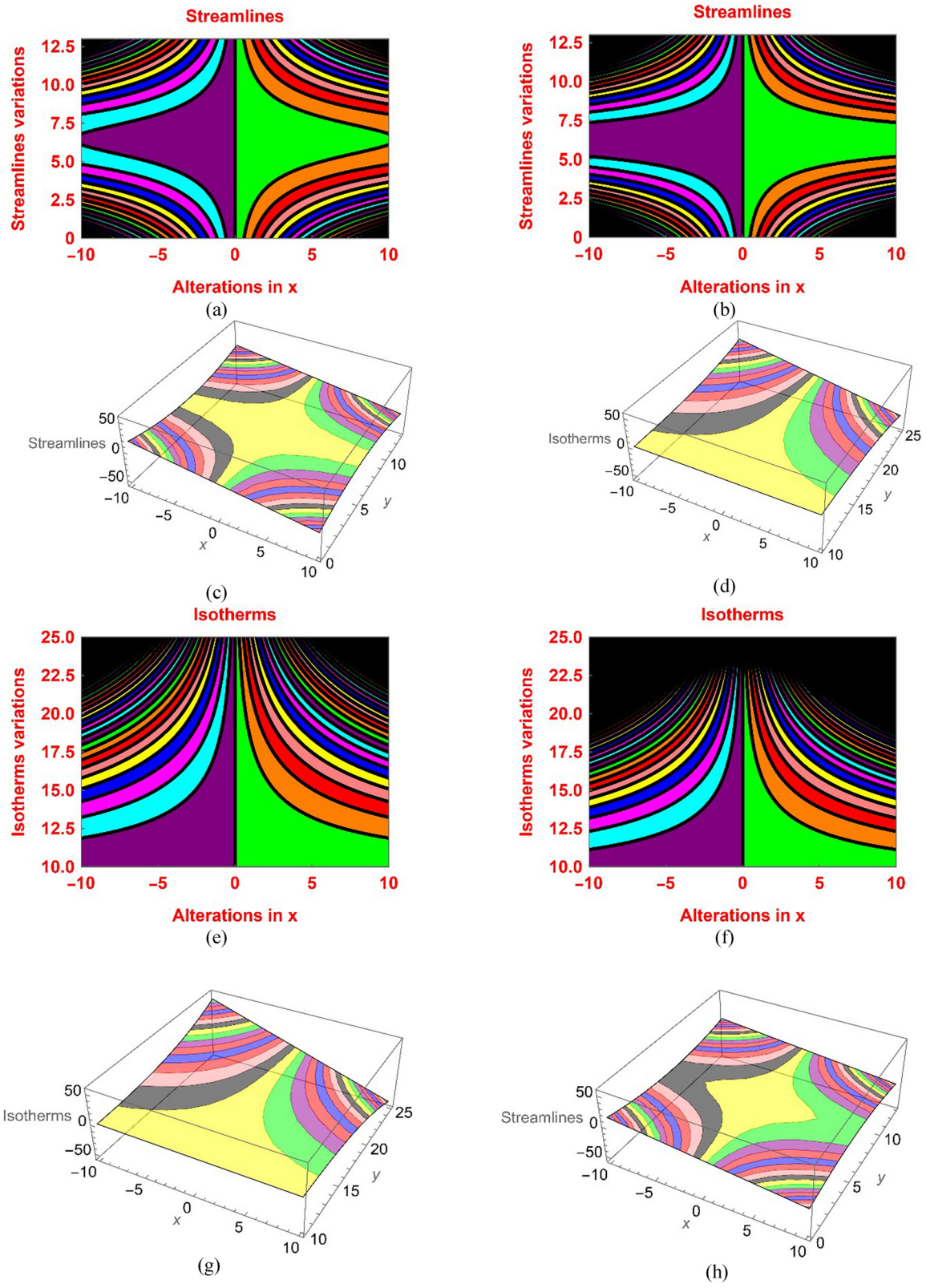

Figure 7: Streamlines and isotherms changes against the model parameters in (a)–(h).

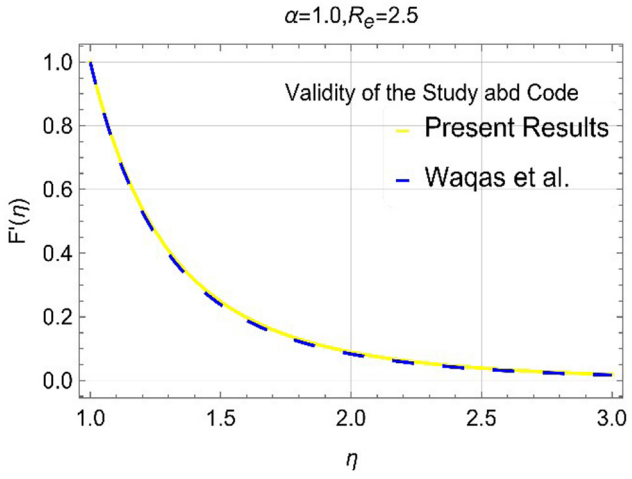

Figure 8: Code and study validation.

the inner part while they become strengthen in the rest of the portion.

The code and study are validated with the results of Waqas *et al.* [2] under restricted parametric values. The result plot for α = 1.0 and Re = 2.5 in Figure 8 and found that both the solutions are well aligned which provides the reliability of the study.

5 Conclusions

Investigation of convectively heated ternary nanofluid past a cylinder is performed. The permeability, radiation, and Reynolds number effects are also included in the problem. It is examined that

- The stronger permeability of the surface (α = 0.1, 0.9, 1.7, 2.5) resists the flow significantly, and a rapid decline is scrutinized for the ternary case while nano and hybrid fluids show slow depreciation in the velocity.
- The Al_2O_3 concentration in the range of 1.0–7.0% provided a considerable increase in the temperature, and dominant trends are observed for the ternary nanofluid.
- The addition of solar radiations (Rd = 0.1, 0.5, 0.9, 1.3) and convective condition (B_i = 0.01, 0.02, 0.03, 0.04) are examined as good physical agents to augment the problem thermal efficiency.
- The skin friction enhances absolutely from −1.07499 to −1.62287 when Re varies from 1.0 to 2.5 and −0.616896 to −0.691989 for α = 1.0, 1.5, 2.0, 2.5.
- The heat gradient enhances from 0.149639 to 0.153987 and 0.420126 to 0.688055 for Re = 1.0, 1.5, 2.0, 2.5 and B_i = 0.5, 1.0, 1.5, 2.0, respectively.

Acknowledgments: The authors extend their appreciation to the Deanship of Scientific Research at Northern Border University, Arar, KSA, for funding this research work through the project number "NBU-FFR-2025-2461-11." Princess Nourah bint Abdulrahman University Researchers Supporting Project number (PNURSP2025R41), Princess Nourah bint Abdulrahman University, Riyadh, Saudi Arabia.

Funding information: This research work was funded by the Deanship of Scientific Research at Northern Border University, Arar, KSA, through the project number "NBU-FFR-2025-2461-11." Princess Nourah bint Abdulrahman University Researchers Supporting Project number (PNURSP2025R41), Princess Nourah bint Abdulrahman University, Riyadh, Saudi Arabia.

Author contributions: Adnan and Waseem Abbas: conceptualization, software, methodology, writing original draft, writing review, and editing. Refka Ghodhbani, Kaouther Ghachem, and Tadesse Walelign: formulation, formal analysis, investigation, software, validation, writing review, and language editing. Yasir Khan, Mehdi Akermi, and Rym Hassani: visualization, formulation, Investigation, writing review, and editing. All authors have accepted responsibility for the entire content of this manuscript and approved its submission.

Conflict of interest: The authors state no conflict of interest.

Data availability statement: All data generated or analyzed during this study are included in this published article.

References

[1] Mishra A. Significance of Thompson and Troian slip effects on Fe_3O_4-$CoFe_2O_4$ ethylene glycol-water hybrid nanofluid flow over a permeable plate. Hybrid Adv. 2024;6:100262. doi: 10.1016/j.hybadv.2024.100262.

[2] Waqas H, Yasmin S, Muhammad T, Imran M. Flow and heat transfer of nanofluid over a permeable cylinder with nonlinear thermal radiation. J Mater Res Technol. 2021;14:2579–85.

[3] Song YQ, Hamid A, Sun TC, Khan MI, Qayyum S, Kumar RN, et al. Unsteady mixed convection flow of magneto-Williamson nanofluid due to stretched cylinder with significant non-uniform heat source/sink features. Alex Eng J. 2022;61(1):195–206.

[4] Nadeem S, Fuzhang W, Alharbi FM, Sajid F, Abbas N, Shafay ASE, et al. Numerical computations for Buongiorno nano fluid model on the boundary layer flow of viscoelastic fluid towards a nonlinear stretching sheet. Alex Eng J. 2022;61(2):1769–78.

[5] Adnan. Heat transfer inspection in [(ZnO-MWCNTs)/water-EG (50:50)]hnf with thermal radiation ray and convective condition over a Riga surface. Waves Random Complex Media. 2022:1–15. doi: 10.1080/17455030.2022.2119300.
[6] Alharbi KAM, Galal AM. Novel magneto-radiative thermal featuring in SWCNT–MWCNT/$C_2H_6O_2$–H_2O under hydrogen bonding. Int J Mod Phys B. 2023;38(2):2450017. doi: 10.1142/S0217979224500176.
[7] Al Rashdi SAA, Ghoneim NI, Amer AM, Megahed AM. Investigation of magnetohydrodynamic slip flow for Maxwell nanofluid over a vertical surface with Cattaneo-Christov heat flux in a saturated porous medium. Results Eng. 2023;19:101293. doi: 10.1016/j.rineng.2023.101293.
[8] Akhter R, Ali MM, Alim MA. Magnetic field impact on double diffusive mixed convective hybrid-nanofluid flow and irreversibility in porous cavity with vertical wavy walls and rotating solid cylinder. Results Eng. 2023;19:101292. doi: 10.1016/j.rineng.2023.101292.
[9] Swain K, Ibrahim SM, Dharmaiah G, Noeiaghdam S. Numerical study of nanoparticles aggregation on radiative 3D flow of maxwell fluid over a permeable stretching surface with thermal radiation and heat source/sink. Results Eng. 2023;19:101208. doi: 10.1016/j.rineng.2023.101208.
[10] Bilal M, Gana S, Muhammad T, Aoudia M, Kolsi L, Ahmad Z. Numerical investigation of tangent hyperbolic stagnation point flow over a stretching cylinder subject to solutal and thermal stratified conditions. J Therm Anal Calorim. 2025;150:2897–907. doi: 10.1007/s10973-024-13631-5.
[11] Zafar M, Khadija R, Ansari MA, Umar K, Kumar A, Khalifa HAE, et al. Analysis of heat generation and viscous dissipation with thermal radiation on unsteady hybrid nanofluid flow over a sphere with double-stratification: Case of modified Buongiorno's model. J Radiat Res Appl Sci. 2024;17(4):101146. doi: 10.1016/j.jrras.2024.101146.
[12] Umar AK, Ahmed N, Basha DB, Mohyud-Din ST, Mahmoud O, Khan I. Numerical investigation of heat transfer in the nanofluids under the impact of length and radius of carbon nanotubes. Open Phys. 2022;20(1):416–30. doi: 10.1515/phys-2022-0040.
[13] Javaid MIM, Imran MA, Khan I, Nisar KS. Natural convection flow of a second grade fluid in an infinite vertical cylinder. Sci Rep. 2020;10:8327. doi: 10.1038/s41598-020-64533-z.
[14] Shah NA, Chung JD, Ahammad NA, Vieru D, Younas S. Thermal analysis of unsteady convective flows over a vertical cylinder with time-dependent temperature using the generalized Atangana–Baleanu derivative. Chin J Phys. 2022;77:1431–49.
[15] Gholinia M, Gholinia S, Hosseinzadeh K, Ganji DD. Investigation on ethylene glycol Nano fluid flow over a vertical permeable circular cylinder under effect of magnetic field. Results Phys. 2018;9:1525–33.
[16] Mishra NK, Khalid AMA, Rahman KU, Eldin SM, Fwaz MZB. Investigation of improved heat transport featuring in dissipative ternary nanofluid over a stretched wavy cylinder under thermal slip. Case Stud Therm Eng. 2023;48:103130. doi: 10.1016/j.csite.2023.103130.
[17] AL-Zahrani AA, Adnan, Mahmood I, Khaleeq RU, Mutasem ZBF, Tag-Eldin E. Analytical study of (Ag–Graphene)/blood hybrid nanofluid influenced by (platelets-cylindrical) nanoparticles and Joule heating *via* VIM. ACS Omega. 2023;8(22):19926–38.
[18] Emam TG. Boundary layer flow over a vertical cylinder embedded in a porous medium moving with non linear velocity. WSEAS Trans Fluid Mech. 2021;16:32–6. doi: 10.37394/232013.2021.16.4.
[19] Rehman A, Bazai R, Achakzai S, Iqbal S. Boundary layer flow and heat transfer of micropolar fluid over a vertical exponentially stretched cylinder. Appl Comput Math. 2015;4(6):424–30.
[20] Ganesh NV, Ganga B, Hakeem AKA, Saranya S, Kalaivanan R. Hydromagnetic axisymmetric slip flow along a vertical stretching cylinder with convective boundary condition. St Petersburg Polytechnical Univ J: Phys Math. 2016;2(4):273–80.
[21] Zokri SM, Syamilah N, Mohamed MKA, Salleh MZ. Mixed convection boundary layer flow over a horizontal circular cylinder in a Jeffrey fluid. AIP Conf Proc. 2017;1842(1):030007. doi: 10.1063/1.4982845.
[22] Javed T, Ahmad H, Ghaffari A. Mixed convection boundary layer flow over a horizontal elliptic cylinder with constant heat flux. J Appl Math Phys. 2015;66:3393–403.
[23] Abbas W, Sayed ME, Mutasem ZBF. Numerical investigation of non-transient comparative heat transport mechanism in ternary nanofluid under various physical constraints. AIMS Math. 2023;8(7):15932–49.
[24] Abdulkhaliq KAM, Adnan, Akgul A. Investigation of Williamson nanofluid in a convectively heated peristaltic channel and magnetic field *via* method of moments. AIP Adv. 2023;13(6):065313. doi: 10.1063/5.0141498.
[25] Cheng CY. Free convection boundary layer flow over a horizontal cylinder of elliptic cross section in porous media saturated by a nanofluid. Int Commun Heat Mass Transf. 2012;39(7):931–6.
[26] Lahonian M, Aminian S, Rahimi MS. Study of MHD mixed convection of different nanofluids due to the inner rotating cylinder saturated with porous media. J Inst Eng (India): Ser C. 2023;104:169–81.
[27] Noreen S, Farooq U, Waqas H, Fatima N, Alqurashi MS, Imran M, et al. Comparative study of ternary hybrid nanofluids with role of thermal radiation and Cattaneo-Christov heat flux between double rotating disks. Sci Rep. 2023;13:7795. doi: 10.1038/s41598-023-34783-8.
[28] Mohanty D, Mahanta G, Shaw S. Irreversibility and thermal performance of nonlinear radiative cross-ternary hybrid nanofluid flow about a stretching cylinder with industrial applications. Powder Technol. 2024;433:119255. doi: 10.1016/j.powtec.2023.119255.
[29] Sarangi MK, Thatoi DN, Shaw S, Azam M, Chamkha AJ, Nayak MK. Hydrothermal behavior and irreversibility analysis of Bödewadt flow of radiative and dissipative ternary composite nanomaterial due to a stretched rotating disk. Mater Sci Eng: B. 2023;287:116124. doi: 10.1016/j.mseb.2022.116124.
[30] Mohanty D, Mahanta G, Byeon H, Vignesh S, Shaw S, Khan MI, et al. Thermo-solutal Marangoni convective Darcy-Forchheimer bio-hybrid nanofluid flow over a permeable disk with activation energy: Analysis of interfacial nanolayer thickness. Open Phys. 2023;21(1):20230119. doi: 10.1515/phys-2023-0119.
[31] Pandey AK, Kumar M. Natural convection and thermal radiation influenceon nanofluid flow over a stretching cylinder in aporous medium with viscous dissipation. Alex Eng J. 2017;56:55–62.
[32] Iqbal AZ, Elattar S, Abbas W, Alhazmi SE, Yassen MF. Thermal enhancement in buoyancy-driven stagnation point flow of ternary hybrid nanofluid over vertically oriented permeable cylinder integrated by nonlinear thermal radiations. Int J Mod Phys B. 2023;37(22):2350215. doi: 10.1142/S0217979223502156.
[33] Mehmood OU, Maskeen MM, Zeeshan A. Electromagnetohydrodynamic transport of Al_2O_3 nanoparticles in ethylene glycol over a convectively heated stretching cylinder. Adv Mech Eng. 2017;9(11):1–8.

[34] Adnan, Alharbi KAM, Bani-Fwaz MZ, Eldin SM, Yassen MF. Numerical heat performance of TiO_2/Glycerin under nanoparticles aggregation and nonlinear radiative heat flux in dilating/squeezing channel. Case Stud Therm Eng. 2023;41:102568. doi: 10.1016/j.csite.2022.102568.

[35] Nadeem A, Sayed ME. Heat transport mechanism in glycerin-titania nanofluid over a permeable slanted surface by considering nanoparticles aggregation and Cattaneo Christov thermal flux. Sci Prog. 2023;106(2). doi: 10.1177/00368504231180032.

[36] Madhukesh JK, Sarris I, Prasannakumara BC. Investigation of thermal performance of ternary hybrid nanofluid flow in a permeable inclined cylinder/plate. Energies. 2023;16(6):2630. doi: 10.3390/en16062630.

[37] Khan M, Zhang Z, Lu D. Numerical simulations and modeling of MHD boundary layer flow and heat transfer dynamics in Darcy-forchheimer media with distributed fractional-order derivatives. Case Stud Therm Eng. 2023;49:103234. doi: 10.1016/j.csite.2023.103234.

[38] Khan M, Imran M. ANN-driven insights into heat and mass transfer dynamics in chemical reactive fluids across variable-thickness surfaces. Heat Transf. 2024;53(8):4551–71.

[39] Khan M, Rasheed A, Anwar MS, Shah STH. Application of fractional derivatives in a Darcy medium natural convection flow of MHD nanofluid. Ain Shams Eng J. 2023;14(9):102093. doi: 10.1016/j.asej.2022.102093.

[40] Khan M, Lu D, Rasool G, Deebani W, Shaaban SM. Fractional numerical analysis of γ-Al_2O_3 nanofluid flows with effective Prandtl number for enhanced heat transfer. J Comput Des Eng. 2024;11(4):319–31.

[41] Aich AW, Sarfraz G, Said NM, Bilal M, Elhag AFA, Hassan AM. Significance of radiated ternary nanofluid for thermal transport in stagnation point flow using thermal slip and dissipation function. Case Stud Therm Eng. 2023;51:103631. doi: 10.1016/j.csite.2023.103631.

[42] Mahmood Z, Rafique K, Khan U, El-Rahman MA, Alharbi R. Analysis of mixed convective stagnation point flow of hybrid nanofluid over sheet with variable thermal conductivity and slip Conditions: A Model-Based study. Int J Heat Fluid Flow. 2024;106:109296. doi: 10.1016/j.ijheatfluidflow.2024.109296.

[43] Ganie AH, Farooq M, Nasrat MK, Muhammad B, Taseer M, Ghachem K. Radiative nanofluid flow over a slender stretching Riga plate under the impact of exponential heat source/sink. Open Phys. 2024;22(1):20240020. doi: 10.1515/phys-2024-0020.